nature physics

LETTERS

PUBLISHED ONLINE: 6 JUNE 2010 | DOI: 10.1038/NPHYS1683

The Widom line as the crossover between liquid-like and gas-like behaviour in supercritical fluids

G. G. Simeoni[1,2], T. Bryk[3,4], F. A. Gorelli[5,6], M. Krisch[7], G. Ruocco[6,8], M. Santoro[5,6]* and T. Scopigno[6,8]

According to textbook definitions[1], there exists no physical observable able to distinguish a liquid from a gas beyond the critical point, and hence only a single fluid phase is defined. There are, however, some thermophysical quantities, having maxima that define a line emanating from the critical point, named 'the Widom line'[2] in the case of the constant-pressure specific heat. We determined the velocity of nanometric acoustic waves in supercritical fluid argon at high pressures by inelastic X-ray scattering and molecular dynamics simulations. Our study reveals a sharp transition on crossing the Widom line demonstrating how the supercritical region is actually divided into two regions that, although not connected by a first-order singularity, can be identified by different dynamical regimes: gas-like and liquid-like, reminiscent of the subcritical domains. These findings will pave the way to a deeper understanding of hot dense fluids, which are of paramount importance in fundamental and applied sciences.

Throughout the past century great effort was devoted to the investigation of the physics of fluid systems: all of their thermodynamical properties in the phase diagram below the critical point are nowadays well known[3]. On the other hand, experimental studies in the supercritical region have been limited so far, owing to technical difficulties. The fluid pressure–temperature (P–T) phase diagram includes a subcritical region with two different phases (liquid and gas, separated by the liquid–vapour coexistence line) and a single-phase supercritical region. Structural and dynamical investigations, aiming to extend the study of the fluid phase diagram well beyond the critical point play a crucial role in many fundamental and applied research fields, such as condensed-matter physics, Earth and planetary science, nanotechnology and waste management[4–8].

From an experimental point of view, the challenge is to close the gap between studies on fluid and solid phases using diamond anvil cell (DAC) techniques[9–12] and studies on hot dense fluids by shock waves[13,14]. As this gap typically overlaps with the supercritical fluid region, it is crucial to track the evolution of transport properties of fluids beyond the critical point. In the specific case of acoustic waves, most of the liquids show the so-called positive dispersion. This is an increase of the speed of sound as a function of wavelength from the continuum limit ($\lambda \to \infty$)—in which the acoustic waves propagate adiabatically—to the short-wavelength limit, that is, on approaching the interparticle distances[15–17]. The ultimate origin of this effect can be traced back to the presence of one (or more) relaxation mechanism(s) interacting with the dynamics of the density fluctuations. The relation between thermodynamics and dynamics, however, is yet to be unveiled, especially at high densities where fluids are well described by simplified potential models (hard-sphere limit; ref. 18).

The possibility of liquid-like behaviour even in the supercritical phase has been advanced by recent inelastic X-ray scattering (IXS) measurements on oxygen[19], presenting a positive dispersion ($\sim$20%) at $T/T_c \sim 2$ and $P/P_c > 100$. On the other hand, this observation contrasts with the gas-like behaviour of deeply supercritical neon ($T/T_c > 6$ and $P/P_c \sim 100$), in which acoustic waves at short wavelengths propagate with the adiabatic sound velocity, and no positive dispersion is observed (see references in ref. 19). This puzzling scenario motivated us to investigate an archetypal model system, argon, along a supercritical, isothermal path from the dense fluid, close to the melting point, far down to the low-density fluid. Using IXS and molecular dynamics simulations we found that the amount of positive dispersion undergoes a transition with a sharp slope crossover on crossing the Widom line, thus marking the borderline between a 'liquid like' and a 'gas like' P–T region. Our findings provide a rationale for recent structural studies, which showed an evolution of the static structure function between a highly correlated liquid-like towards a weakly correlated gas-like structure[18].

Details on the experimental IXS and high-pressure techniques are included in refs 19 and 20. The molecular dynamics simulations were carried out in the standard microcanonical ensemble for a model system of 2,000 particles interacting through an *ab initio* potential (see the Methods section). All of the calculated thermodynamic quantities agree with the values provided by the National Institute of Standards and Technology (NIST) source[21], where available (that is, at $P \leq 1$ GPa), within 1%. IXS and molecular dynamics spectra ($T = 573$ K) are reported in Fig. 1, as a function of pressure, and at selected momentum transfer values $Q = 2\pi/\lambda$. The experimental and simulated spectra are in very good agreement and show two inelastic peaks corresponding to the acoustic excitations. With increasing Q, these peaks shift towards higher frequencies and continuously broaden, and ultimately merge into the central peak. At a given Q, conversely, we observe an increase of the acoustic excitation frequency with pressure, showing the increase of the sound velocity.

The wavelength-dependent sound velocity $c(Q)$ can be obtained from the density fluctuations' autocorrelation spectrum $S(Q,\omega)$

[1]Technische Universität München, Forschungsneutronenquelle Heinz, Maier-Leibnitz FRM II, D-85747 Garching, Germany, [2]Technische Universität München, Physik Department E13, D-85748 Garching, Germany, [3]Institute for Condensed Matter Physics, National Academy of Sciences of Ukraine, UA-79011 Lviv, Ukraine, [4]National Polytechnic University of Lviv, UA-79013 Lviv, Ukraine, [5]LENS, European Laboratory for Non Linear Spectroscopy, Sesto Fiorentino, I-50019 Firenze, Italy, [6]IPCF-CNR, UOS Roma, I-00185 Roma, Italy, [7]European Synchrotron Research Facility, F-38043 Grenoble, France, [8]Dipartimento di Fisica, Università di Roma 'La Sapienza', I-00185 Roma, Italy. *e-mail: santoro@lens.unifi.it.

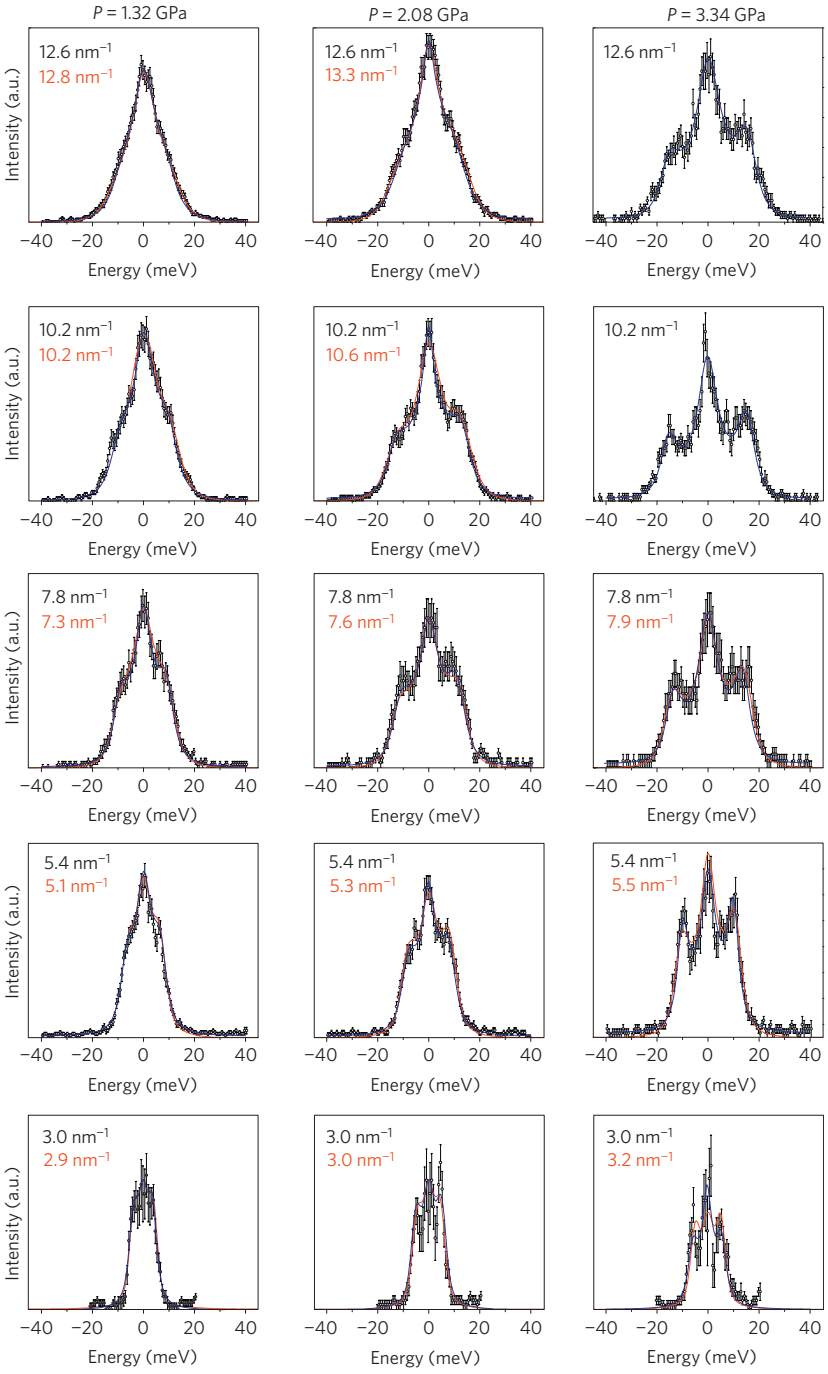

Figure 1 | IXS spectra of supercritical argon at $T = 573$ K. Dots with error bars: experimental spectra. The three columns correspond to the three different pressures 1.32, 2.08 and 3.34 GPa, and rows report spectra taken at the indicated Q values (in black). Blue line: model $S(Q,\omega)$ convoluted with the instrumental resolution function and fitted to the measured spectra. Red line: $S(Q,\omega)$ as obtained from the molecular dynamics simulations and convoluted with the instrumental resolution function. The Q values of the reported molecular dynamics spectra, indicated in red, are close to the ones of the IXS spectra. The error bars mark the signal-related, statistical errors.

(refs 15,17), which in turn is obtained from the IXS spectrum or can be evaluated in the molecular dynamics simulation from the atomic trajectories. Specifically, $c(Q) = \omega(Q)/Q$, with $\omega(Q)$ being the maximum of the current autocorrelation function $J(Q,\omega) = \omega^2/Q^2 * S(Q,\omega)$. The adiabatic, $\lambda \to \infty$ limit of the sound velocity, indicated as c_S, is defined as $c_S = \lim_{Q\to 0}[\sqrt{\gamma(Q)k_B T/MS(Q)}]$ (refs 15,17), where k_B, M and T are the Boltzmann constant, the atomic mass and the temperature, respectively, and $\gamma(Q)$ and $S(Q)$ are the wavelength-dependent specific-heat ratio and the static structure factor, which can be easily determined by the molecular dynamics simulations. In Fig. 2 (upper panels) we report, for the three investigated pressures, the dispersion curves $\hbar Qc(Q)$ as determined by IXS and molecular dynamics and the 'adiabatic dispersion' $\hbar Q\sqrt{\gamma(Q)k_B T/MS(Q)}$. The lower panels report the corresponding $c(Q)$, $\sqrt{\gamma(Q)k_B T/MS(Q)}$ and c_S. The maximum of the ratio $c(Q)/c_S$ defines the amount of positive dispersion, which turns out to decrease on decreasing the pressure, in both the IXS experiment and molecular dynamics simulations (Fig. 3). The extension of this observation below 1 GPa is surprising. This pressure region is experimentally difficult to explore with the

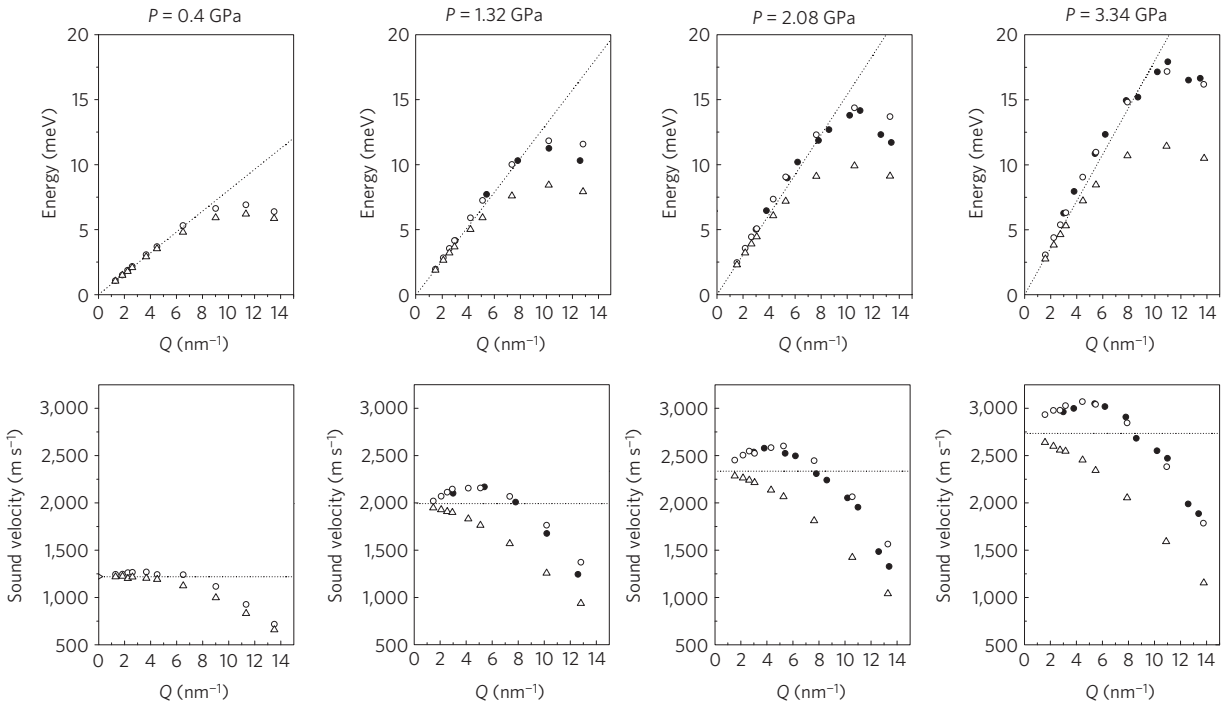

Figure 2 | Energy and sound-velocity dispersions. Energy (upper panels) and sound-velocity (lower panels) dispersion curves of supercritical argon at $T = 573$ K and pressures equal to 0.4, 1.32, 2.08 and 3.34 GPa. Energy dispersion curves: IXS (filled circles) and molecular dynamics (open circles) values of $\hbar\omega(Q) = \hbar Qc(Q)$, where $\omega(Q)$ are the maxima of the current autocorrelation function; molecular dynamics values of the adiabatic sound propagation $\hbar Q\sqrt{\gamma(Q)k_BT/MS(Q)}$ (open triangles) and the $\hbar c_S Q$ line. Sound-velocity dispersion: $c(Q)$ (filled and open circles for IXS and molecular dynamics, respectively) and $\sqrt{\gamma(Q)k_BT/MS(Q)}$ (open triangles, molecular dynamics). Horizontal lines: adiabatic sound velocity c_S. The triangle at $Q = 0$ nm^{-1} in the first panel, at $P = 0.4$ GPa, represents c_S as obtained by the NIST database[21].

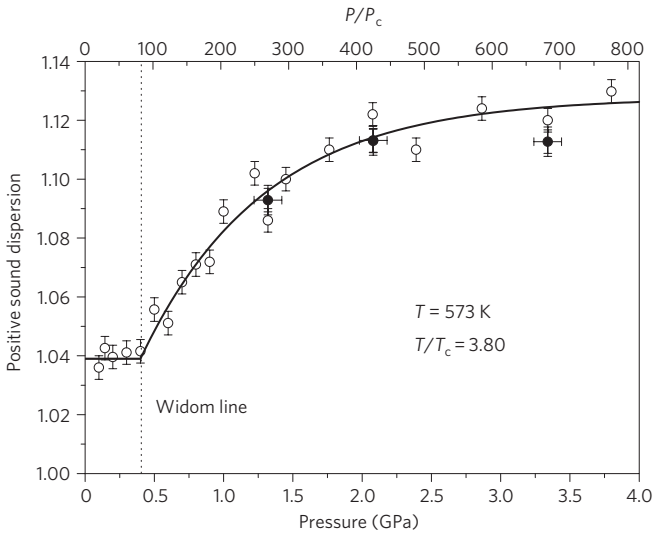

Figure 3 | Positive sound dispersion, that is, the maximum of the ratio $c(Q)/c_S$ as a function of pressure at 573 K. Dotted line: point on the extrapolated Widom line at 573 K, see text and Fig. 4. The filled and open circles indicate the positive sound dispersion as obtained from the IXS experimental data and from the molecular dynamics simulations, respectively. Two lines, as a guide for the eye, have been fitted to the whole set of points. The vertical error bars are due to two independent sources of uncertainty: (1) the error on the estimation of the maximum of the apparent sound dispersion (bottom panels of Fig. 2) from the fit with a polynomial function, and (2) the error on the adiabatic sound velocity as derived from the simulations. The horizontal error bars are related to the fitting procedure of the fluorescence peaks of the optical gauge sensors used for the pressure measurement.

DAC, owing to the exceedingly low scattering signal at low densities, the limited accuracy in controlling the pressure and the high risk of sample loss. On the other hand, on the basis of the very good agreement between IXS and molecular dynamics, a clear picture is obtained combining the results of the two techniques (Fig. 3): the 13% positive dispersion close to the melting line decreases on decreasing pressure to about 4%, with a sharp slope cutoff at 0.4 GPa. This can be rationalized within a two-relaxation-process scenario: the structural process, representing the viscoelastic behaviour of any liquid, and a microscopic relaxation, related to nearest-neighbours interaction, specifically to the non-plane-wave nature of instantaneous vibrational eigenmodes of the system. Both of these processes are a source of positive dispersion. In agreement with previous experimental studies[22,23] and recent theoretical efforts, our study shows that the latter mechanism turns out to be weakly dependent on the thermodynamic state of the system when compared with the structural relaxation, giving rise in the present case to a 4% baseline of positive dispersion in the explored P–T range. Most importantly, we detail in this work the evolution of the structural relaxation in the supercritical region. Remarkably, the crossover of the positive dispersion unveils a partition of the phase diagram in deep supercritical conditions. We note that this crossover is far away from the critical isochore. In fact, in terms of density, it occurs at 1.18 g cm^{-3} (equation of state from the NIST database[21]), which is very close to the density of the liquid at the triple point, 1.4168 g cm^{-3}, whereas the critical density is equal to 0.5357 g cm^{-3}. The partition of the phase diagram marked by the crossover is particularly significant because the peak of the constant-pressure specific heat C_P becomes broader and broader beyond the critical point: the Widom line ceases to exist around $P/P_c = 30.1$ and $T/T_c = 3, 12$ (ref. 21). On the other hand, the dynamical crossover that we measure in this work on the positive dispersion provocatively lies on the Widom line extrapolation

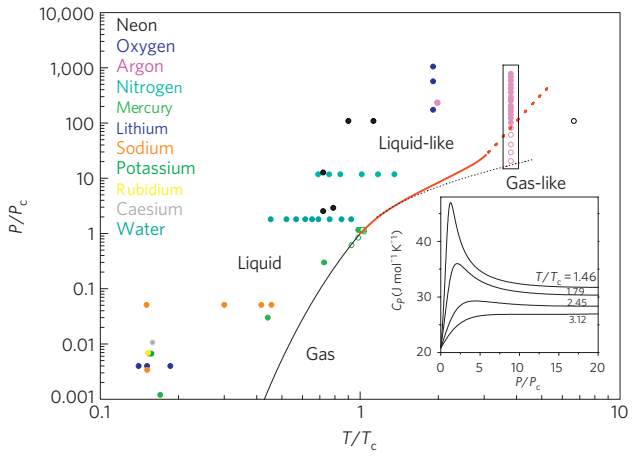

Figure 4 | Sketch of the (P/P_c, T/T_c) plane. Red line: the Widom line of argon obtained from the NIST database (continuous)[21] up the highest temperature where a maximum in C_P versus P can still be identified ($T = 470$ K; $T/T_c = 3.12$), as shown in the inset, and extrapolated (dotted) above this temperature. Black line: best fit of the average of the liquid–vapour coexistence lines for argon, neon, nitrogen and oxygen using the Plank–Riedel equation[19]. Black, dotted line: argon critical isochore obtained from the NIST database[21]. The dots with different colours correspond to different investigated systems (this study, and also ref. 19 and references therein). Isothermal, experimental and molecular dynamics simulation data on argon are reported in pink inside a rectangle. The extra point on argon outside the rectangle has been obtained in another experiment at room temperature[20]. Open points represent cases where the positive dispersion of the sound velocity exhibits low values, full points cases where there is a clear signature of high positive dispersion.

deep inside the supercritical region. Therefore, our result allows extending the notion of the Widom line, and, most importantly, to ascribe to it a completely new essence (Fig. 4). Indeed, the Widom line was originally defined within the thermodynamic frame to represent the fate of the subcritical behaviour (divergence) of C_P beyond the critical point. Whereas for subcritical fluids along the coexistence line all thermodynamical response functions simultaneously diverge, in the case of supercritical fluids the notion of divergence is replaced by that of a maximum and one can identify a line for each response function (the Widom line in the case of C_P), converging in the neighbourhood of the critical point[24–26]. These lines are not connected to some criticalities of any thermodynamic quantities, in agreement with the textbook definition of a unique fluid phase. Our result, however, demonstrates that the Widom line identifies a well-defined partition between two completely different dynamical behaviours reminiscent of gas and liquid dynamic properties, surviving even where the Widom line itself ceases to exist in its standard definition.

In Fig. 4 we report the Widom line in a reduced $P/P_c - T/T_c$ phase diagram, obtained from C_P data[21]. Interestingly, it can be seen how the Widom line smoothly extends the Plank–Riedel equation for the liquid–gas coexistence line of noble gases[19] beyond the critical point. We also report the thermodynamical points investigated in this study. The filled (open) dots indicate points with pressure-dependent (independent), relatively high (low) positive dispersion. The two sets of points are separated by the Widom line. It is then clear that the phase diagram is divided into two supercritical regions: liquid-like and gas-like, which have to be considered as extensions of the subcritical liquid and gas phases, respectively. The figure also shows literature P–T points where the positive dispersion has been checked, on a variety of fluid systems at subcritical or slightly supercritical conditions. A high positive dispersion is actually present only in the liquid and liquid-like regions, whereas the positive dispersion is low or absent in the gas and gas-like regions. This puts our findings on a very general ground.

We speculate that the positive dispersion may play the role of an order parameter: from the continuity of the pressure behaviour (and discontinuity in the slope) underlined in Fig. 3, a phase transition is suggested to take place at the Widom line, in analogy to the subcritical behaviour. This is the same interplay between dynamics and thermodynamics described by the liquid–vapour coexistence line in the subcritical fluid region, thus supplying the first fundamental insight into the correspondence between subcritical and supercritical fluid behaviour and allowing recent X-ray diffraction measurements to be put in perspective[18]. Consequently, the Widom line appears as the eligible thermodynamic indicator of the liquid-like to gas-like dynamical crossover. These findings cast the notion of supercritical fluid under a new perspective, opening up new territory for which there is at present no theoretical framework. We expect that the revealed relation between thermodynamics and the viscoelastic behaviour of elastic moduli in hot dense fluids will allow major breakthroughs in diverse areas. These include the rich physics of planetary systems, the quest for new solvation techniques demanded by nanotechnologies and the validation of seismological models based on the thermophysical properties of geophysically relevant materials.

Methods

The experiment was carried out on the beamline ID28 at the ESRF, with an energy resolution of 3.0 meV. The DAC was placed into a vacuum chamber to minimize and control the empty cell contributions to the scattering signal[20]. The pressure was measured *in situ* by the wavelength shift of the ruby and SrB_4O_7:Sm^{2+} fluorescence peaks. The temperatures were determined by a thermocouple placed very close to one diamond. The detailed description of the beamline set-up, the vacuum chamber and the sample loading procedure can be found in refs 19 and 20.

The intensity of the IXS spectra as a function of exchanged momentum Q and frequency ω, $I(Q,\omega)$, depends on the classical dynamic structure factor $S(Q,\omega)$ as:

$$I(Q,\omega) = \int \frac{\hbar\omega'/KT}{1-e^{-\hbar\omega'/KT}} S(Q,\omega')R(\omega-\omega')d\omega' \quad (1)$$

The first factor in the integral is the Bose factor, accounting for the quantum population effect, and the integral represents the convolution with the instrumental resolution $R(\omega)$. In the memory function framework, $S(Q,\omega)$ can be expressed as[15,17]:

$$\frac{S(Q,\omega)}{S(Q)} = \frac{\omega_0^2(Q)\tilde{M}'(Q,\omega)/\pi}{[\omega^2-\omega_0^2(Q)-\omega\tilde{M}''(Q,\omega)]^2+[\omega\tilde{M}'(Q,\omega)]^2} \quad (2)$$

where $\tilde{M}(Q,\omega) = \tilde{M}'(Q,\omega) + i\tilde{M}''(Q,\omega)$ is the Laplace transform of the memory function. In the time domain, the memory function can be written as:

$$M(Q,t) = [\gamma(Q)-1]\omega_0^2(Q)e^{-\gamma(Q)D_T(Q)Q^2t} + \Delta_\alpha^2(Q)e^{-t/\tau_\alpha(Q)} \quad (3)$$

where $\gamma(Q)$ and $D_T(Q)$ are the Q-dependent specific-heat ratio and thermal diffusivity, respectively. Furthermore, $\omega_0 = \sqrt{k_B T/MS(Q)}$, where k_B, M and T are the Boltzmann constant, the atomic mass and the temperature, respectively, and $S(Q)$ is the static structure factor. Then, $\Delta_\alpha^2(Q) = (c_\infty^2 - c_S^2)Q^2$ is the strength of the structural relaxation process, with c_S and c_∞ being the low- and the high-frequency sound velocity, respectively. Combining equations (1)–(3), we obtain the best fit plotted in Fig. 1 (blue line). Free-fit parameters were $\Delta_\alpha(Q)$ and $\tau_\alpha(Q)$. $D_T(Q)$, $\gamma(Q)$ and $\omega_0(Q)$ (that is, the $S(Q)$) were set to the values obtained by the molecular dynamics simulations. The molecular dynamics simulations were carried out at different densities at $T = 573$ K (the corresponding pressures were obtained from NIST data (ref. 21) up to 1 GPa and, above this pressure, by means of the expression: $n(\mathrm{g\,cm^{-3}}) = A + B\cdot\log(P(\mathrm{GPa}))$, where $A = 1.5795\ \mathrm{g\,cm^{-3}}$ and $B = 1.0075\ \mathrm{g\,cm^{-3}}$) in the standard microcanonical ensemble for a model system of 2,000 particles interacting through an *ab initio* potential[27,28] with 12 Å cutoff radius. We checked, at a few densities, that the same results are obtained by more complex simulations with 4,000 particles and 20 Å cutoff radius. The production runs were of 600,000 time steps, each one of 2 fs, and the energy drift over each production run was not higher than 0.2%. All of the calculated thermodynamic quantities agree with the values provided by the NIST source[21], where available (that is, at $P \leq 1$ GPa), within 1%. For the purpose of the analysis of collective dynamics we sampled the following five dynamic variables: number density $n(Q,t)$, density of longitudinal momentum $J_L(Q,t)$, energy density $e(Q,t)$ and first time derivatives of $J_L(Q,t)$ and $e(Q,t)$. The dynamic variables were saved for each sixth configuration and

used later for calculations of dynamic structure factors $S(Q,\omega)$ and current spectral functions $C_L(Q,\omega)$ as well as generalized thermodynamic quantities such as specific heats $C_P(Q)$ and $C_V(Q)$, their ratio $\gamma(Q)$ and linear thermal expansion coefficient $\alpha_T(Q)$ using well-known expressions[29,30]. It was proved in numerous simulations of Lennard-Jones fluids, liquid metals, molten salts and water that this is the most reliable way to estimate generalized thermodynamic quantities and macroscopic values for liquids directly from molecular dynamics simulations.

Received 14 January 2010; accepted 27 April 2010; published online 6 June 2010

References

1. Medard, L. *Gas Encyclopaedia* (Elsevier, 1976).
2. Widom, B. in *Phase Transitions and Critical Phenomena,* Vol. 2 (eds Domb, C. & Green, M. S.) (Academic, 1972).
3. Zemanski, M. W. *Heat and Thermodynamics* (MacGraw-Hill, 1968).
4. McMillan, P. F. A stranger in paradise. *Science* **310,** 1125–1126 (2005).
5. Sanloup, C. *et al.* Retention of xenon in quartz and Earth's missing xenon. *Science* **310,** 1174–1177 (2005).
6. Johnston, K. P. & Shah, P. S. Making nanoscale materials with supercritical fluids. *Science* **303,** 482–483 (2004).
7. De Simone, J. M. Practical approaches to green solvents. *Science* **296,** 799–803 (2002).
8. Kendall, J. L., Canelas, D. A., Young, J. L. & De Simone, J. M. Polymerizations in supercritical carbon dioxide. *Chem. Rev.* **99,** 543–563 (1999).
9. Eggert, J. H., Weck, G., Loubeyre, P., Mezouar, M. & Hanfland, M. Quantitative structure factor and density measurements of high-pressure fluids in diamond anvil cells by X-ray diffraction: Argon and water. *Phys. Rev. B* **65,** 174105 (2002).
10. Goncharenko, I. & Loubeyre, P. Neutron and X-ray diffraction study of the broken symmetry phase transition in solid deuterium. *Nature* **435,** 1206–1209 (2005).
11. Eremets, M. I., Gavriliunk, A. G., Trojan, I. A., Dzivenko, D. A. & Boehler, R. Single-bonded cubic form of nitrogen. *Nature Mater.* **3,** 558–563 (2004).
12. Santoro, M. *et al.* Amorphous silica-like carbon dioxide. *Nature* **441,** 857–860 (2006).
13. Chau, R., Mitchell, A. C., Minich, R. W. & Nellis, W. J. Metallization of fluid nitrogen and the Mott transition in highly compressed low-Z fluids. *Phys. Rev. Lett.* **90,** 245501 (2003).
14. Weir, S. T., Mitchell, A. C. & Nellis, W. J. Metallization of fluid molecular hydrogen at 140 GPa (1.4 Mbar). *Phys. Rev. Lett.* **76,** 1860–1863 (1996).
15. Boon, J. P. & Yip, S. *Molecular Hydrodynamics* (McGraw-Hill, 1980).
16. Scopigno, T., Balucani, U., Ruocco, G. & Sette, F. Evidence of two viscous relaxation processes in the collective dynamics of liquid lithium. *Phys. Rev. Lett.* **85,** 4076–4079 (2000).
17. Scopigno, T., Ruocco, G. & Sette, F. Microscopic dynamics in liquid metals: The experimental point of view. *Rev. Mod. Phys.* **77,** 881–933 (2005).
18. Santoro, M. & Gorelli, F. A. Structural changes in supercritical fluids at high pressures. *Phys. Rev. B* **77,** 212103 (2008).
19. Gorelli, F. A., Santoro, M., Scopigno, T., Krisch, M. & Ruocco, G. Liquid-like behaviour of supercritical fluids. *Phys. Rev. Lett.* **97,** 245702 (2006).
20. Gorelli, F. A. *et al.* Inelastic x-ray scattering from high pressure fluids in a diamond anvil cell. *Appl. Phys. Lett.* **94,** 074102 (2009).
21. NIST Chemistry WebBook, http://webbook.nist.gov/chemistry/.
22. Ruocco, G. *et al.* Relaxation processes in harmonic glasses? *Phys. Rev. Lett.* **84,** 5788–5791 (2000).
23. Scopigno, T., Sette, F., Ruocco, G. & Viliani, G. Evidence of short-time dynamical correlations in simple liquids. *Phys. Rev. E* **66,** 031205 (2002).
24. Xu, L. *et al.* Relation between the Widom line and the dynamic crossover in systems with a liquid–liquid phase transition. *Proc. Natl Acad. Sci. USA* **102,** 16558–16562 (2005).
25. Kumar, P. *et al.* Breakdown of the Stone–Einstein relation in supercooled water. *Proc. Natl Acad. Sci. USA* **104,** 9575–9579 (2006).
26. Liu, L., Chen, S-H., Faraone, A., Yen, C-W. & Mou, C-Y. Pressure dependence of fragile-to-strong transition and a possible second critical point in supercooled confined water. *Phys. Rev. Lett.* **95,** 117802 (2005).
27. Woon, D. E. Accurate modeling of intermolecular forces: A systematic Moller–Plesset study of the argon dimer using correlation consistent basis sets. *Chem. Phys. Lett.* **204,** 29–35 (1993).
28. Bomont, J. M., Bretonnet, J. L., Pfleiderer, T. & Bertagnolli, H. Structural and thermodynamic description of supercritical argon with *ab initio* potentials. *J. Chem. Phys.* **113,** 6815–6821 (2000).
29. De Schepper, I. M. *et al.* Hydrodynamic time correlation functions for a Lennard-Jones fluid. *Phys. Rev. A* **38,** 271–287 (1988).
30. Mryglod, I. M., Omelyan, I. P. & Tokarchuk, M. V. Generalized collective modes for the Lennard-Jones fluid. *Mol. Phys.* **84,** 235–259 (1995).

Acknowledgements

We acknowledge the ESRF for provision of beam time at ID28, and we thank D. Gambetti, M. Hoesch, J. Serrano-Gutierrez, A. Beraud and A. Bossak for fruitful discussions and assistance during the experiments. F.A.G. and M.S. have been supported by the European Community, under Contract No. RII3-CT2003-506350. T.S. has received financial support from the European Research Council under the European Community's Seventh Framework Program (FP7/2007-2013)/ ERC grant Agreement No. 207916.

Author contributions

F.A.G., M.S. and T.S. proposed the research, did the project planning, the experimental work, contributed to data analysis and interpretation, and wrote the paper. T.B. carried out the molecular dynamics simulations and contributed to data interpretation. G.G.S. and G.R. contributed to data analysis and interpretation, and to writing the paper. M.K. contributed to the experimental work and to data interpretation.

Additional information

The authors declare no competing financial interests. Reprints and permissions information is available online at http://npg.nature.com/reprintsandpermissions. Correspondence and requests for materials should be addressed to M.S.